Journal of Building Engineering 72 (2023) 106623

Contents lists available at ScienceDirect

Journal of Building Engineering

journal homepage: www.elsevier.com/locate/jobe

Pyroclastic volcanic ash as a potential precursor of alkali-activated binders – A case study from Tajogaite (La Palma, Canary Islands) volcano eruption

Jofre Mañosa [a], Jesús Serrano-Conte [a], Alex Maldonado-Alameda [a], Meritxell Aulinas [b], Josep M. Chimenos [a,*]

[a] Departament de Ciència de Materials i Química Física, Universitat de Barcelona, Martí i Franquès 1, 08028, Barcelona, Spain
[b] Departament de Mineralogia, Petrologia i Geologia Aplicada, Universitat de Barcelona, Martí i Franquès s/n, 08028, Barcelona, Spain

ARTICLE INFO

Keywords:
Alkali-activated binders
Alkaline activation
Waste valorisation
Sustainable cements
Volcanic ash

ABSTRACT

The volcanic eruption of Tajogaite in La Palma (Canary Islands, Spain) produced approximately 200 Mm^3 of fine lapilli and ash. Using this volcanic ash (VA) to produce alkali-activated binders (AABs) fosters a sustainable approach to binder manufacturing, aligning with the principles of a circular economy and reducing reliance on non-renewable resources. The feasibility of using VA as a sole precursor for the formulation of sustainable AABs was evaluated based on its composition and physical-chemical properties. To this end, a comprehensive physicochemical characterization of VA was carried out and the physical, mechanical, and environmental properties of the binders formulated were analyzed. The physical-chemical analysis reveals the neoformation of typical secondary reaction products, such as NASH and (C,N)ASH gels. The microstructure analysis reveals that the AABs formulated using 6 M and 8 M NaOH activator solutions contain homogeneously dispersed unreacted VA particles within the binder matrix, providing increased cohesion and mechanical strength. The highest compressive resistance of AABs formulated using only VA as the precursor was achieved with a 6 M NaOH activator solution and a curing temperature of 60 °C, reaching a strength of 16 MPa. Although alkaline activation enhances the release of some metals and metalloids contained in the VA, the study of the environmental requirements at the end of the life cycle of the formulated AABs allows them to be classified as non-hazardous materials.

1. Introduction

The volcanic eruption of the Tajogaite cone on the Cumbre Vieja ridge, located on the island of La Palma (Canary Islands, Spain), took place in September 2021. It is estimated that the volcanic activity, which lasted 85 days, expelled around 200 Mm^3 of total pyroclastic deposits and lavas in the different flows [1]. In addition, an estimated 45 Mm^3 of pyroclastic material, consisting mainly of fine lapilli and ash, was emitted during the eruption and deposited all over La Palma, sometimes reaching the neighbouring islands [2]. On the one hand, the accumulation of ballistic projection pyroclasts, mainly bombs (>64 mm in size) and lapilli (>2 to <64 mm in size), around the eruptive vents, was responsible for the construction of the central volcanic cone. On the other hand, horizontally dispersed pyroclasts, including lapilli and ash (<2 mm in size), formed deposits that uniformly covered the previous terrain, especially

* Corresponding author.
E-mail address: chimenos@ub.edu (J.M. Chimenos).

https://doi.org/10.1016/j.jobe.2023.106623
Received 26 March 2023; Received in revised form 17 April 2023; Accepted 19 April 2023
Available online 20 April 2023

on the southern slope of the volcano due to the prevailing wind direction, where thickness up to 3 m were measured [1,3].

On the other hand, Portland Cement (PC) is the most commonly used binder in the formulation of construction materials. Approximately 4215 Mt of PC were produced worldwide in 2018, with global demand expected to increase by around 18% by 2030 [4]. The production of PC has become one of the world's primary anthropogenic sources of CO_2 emissions, due to its high consumption, and the thermal processes involved in the manufacture of clinker. In this sense, the cement industry is estimated to generate 5–7% of global CO_2 emissions and consume 3% of the world's primary energy [5]. Therefore, the cement industry must identify alternative binders that require less energy and produce less greenhouse gas emissions, and whose use can partially or totally replace PC. In this regard, alkali-activated binders (AABs) are one of the most promising options due to their high performance and low carbon footprint [6,7]. Furthermore, a wide range of industrial waste and/or kilometre-zero aluminosilicates-rich materials can be used as precursors in the formulation of AABs, promoting the manufacture of sustainable binders in the framework of a circular economy, leading to a reduction in the exploitation of natural resources.

Additionally, given the limited natural resources and lack of land transportation, the supply of materials and energy resources to an island can become a critical issue. Therefore, the problem of the production and/or supply of PC can be aggravated in an island environment, which may see increased energy costs and environmental emissions associated with the consumption of resources from mainland suppliers. Thus, the unavailability of suitable construction materials is a challenge to constructing and maintaining buildings on small islands. Therefore, on a small island, finding alternative resources that contemplate lower energy consumption and more sustainable processes is more urgent. In this regard, the substitution of imported building supplies for locally manufactured or locally sourced materials, based on more sustainable processes, should be promoted while contributing to the development of the local economy [8]. Accordingly, for the island of La Palma (Canary Islands, Spain), the use of pyroclastic materials produced by the volcanic eruption can be helpful for the rapid restoration of the affected area, with construction and building being one of the sectors with the greatest need for resources. In addition, using pyroclastic deposits as secondary raw material has economic benefits due to the low-cost mining and a limited negative environmental impact [9].

Natural or artificial pozzolans have been commonly used as supplementary cementitious materials to partially replace PC reducing CO_2 emissions and improving several properties [10,11]. The main components of pozzolans for cementitious materials are silica (SiO_2) and alumina (Al_2O_3), which in alkali media are able to form stable silicate and/or aluminosilicate compounds with binder properties. In this regard, volcanic pozzolans are known as pyroclastic materials suitable for partial replacement of PC in the manufacture of paste, mortar or concrete [12]. Volcanic ash (VA), which is included among volcanic pozzolans, does not require much pre-treatment to increase its pozzolanic activity (e.g. grinding) due to its smaller particle size [13]. VA, as it is, has been successfully used as supplementary cementitious material partially replacing PC (blended cement), and more recently, as a precursor for sustainable binding materials such as alkali-activated binders (AABs) [9,11,12,14–19]. The scientific and technical interest in using VA for the formulation of AABs has increased since 2012 [20], as interest in the recirculation of secondary resources has also increased. In the case of the VA from the eruption of the Cumbre Vieja ridge, it has occupied a large part of the island's territory and must be collected from infrastructures and buildings, generating a problem regarding its management. Therefore, its possible application in the construction field becomes an opportunity to manage and, in turn, value this resource.

Although there are numerous references to using VA as precursors in the formulation of AABs, the composition and physicochemical properties of VA depend on their origin, environmental conditions of their location and weathering time [13]. Accordingly, the main target of this research is to study VA from the Cumbre Vieja ridge eruption (La Palma, Canary Islands) to evaluate its potential use as a sole precursor in the formulation of sustainable alkali-activated binders. The physicochemical characterization of VA and the physical, mechanical, and environmental properties of pastes formulated have been studied.

2. Materials and methods

2.1. Materials

The volcanic ash (VA) used as a raw material for the formulation of AABs was collected and supplied by members of the Institute for Environmental Studies and Natural Resources (Instituto de Estudios Ambientales y Recursos Naturales, I-UNAT) of the University of Las Palmas de Gran Canaria, during different periods of the volcanic eruption. In particular, the tephra samples were collected in the vicinity of the El Paso village, located on the western flank of the Cumbre Vieja rift zone of La Palma island (Canary Islands, Spain).

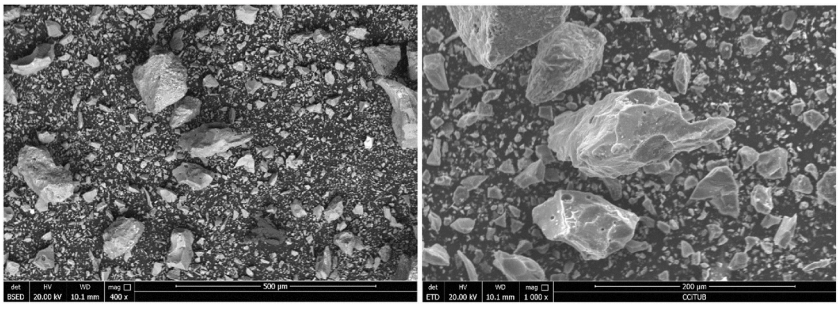

Fig. 1. Volcanic ash (VA) from Cumbre Vieja ridge (La Palma, Canary Islands) as received.

Different solutions of NaOH and Na_2SiO_3 (water glass) were used as alkaline activators in the preliminary studies and later during the formulation of the AABs. Concentrations of NaOH 4 M ($\rho = 1.16$ g cm^{-3}), 6 M ($\rho = 1.20$ g cm^{-3}), and 8 M ($\rho = 1.24$ g cm^{-3}) were prepared using NaOH pearls (Labbox Labware S.L.; purity >98%) dissolved in deionised water. The Na_2SiO_3 solution with mass fraction $SiO_2/Na_2O = 2.4–2.6$ ($\rho = 1.45–1.48$ g cm^{-3}) was provided by LabKem.

2.2. Volcanic ash characterization

Fig. 1 shows the collected sample micrograph as received, obtained through scanning electron microscopy (SEM) ESEM FEI Quanta 200 device. The VA, which presented a black powdery appearance with a glassy vesicular structure, is mainly formed by juvenile fragments (pyroclasts derived directly from the erupting magma) with minor lithic particles (fragments of non-volcanic rocks or from volcanic rocks not related to the erupting volcano) and free crystals. In turn, juvenile fragments correspond to volcanic glass in the form of tachylyte (blackish-coloured) and sideromelane (golden brown-coloured) scoriae [21,22]. About 2 kg of VA of the homogenised sample was dried at 105 °C overnight and subsequently crushed and ground in a RETSCH RS100 jaw crusher to increase the specific surface area of the precursor and obtain a particle size powder below 80 μm [15].

The VA's particle size distribution (PSD), as received and after the grinding process, was determined using a Beckman Coulter LS13 320 particle size analyser (Fig. 2). The particle size significantly decreased after the milling process ($d_{90} = 88$ μm and a $d_{50} = 36$ μm) compared with the initial VA ($d_{90} = 250$ μm). In addition, the specific surface area (BET) was measured with a Micrometrics Tristar 3000 porosimeter, revealing a notable increase in the milled VA (5.61 m^2 g^{-1}) compared with the initial VA (1.82 m^2 g^{-1}) received, which denotes a higher reactivity potential.

The elemental composition of VA was evaluated by X-ray fluorescence (XRF) analysis with a Panalytical Philips PW 2400 sequential X-ray spectrophotometer equipped with UniQuant® V5.0 software. Major, minor and trace elements expressed as their most stable oxides are given in Table 1.

The analyzed VA are alkaline mafic rocks classified as basanites [23] with similar compositions to those reported on lavas of the 2021 Tajogaite eruption [24] and are comparable to the chemical compositions of VA collected from other mafic alkaline volcanic eruptions worldwide [13]. The presence of Si, Al, and Ca, essential elements for forming different AABs' phases (CSH, NASH and/or CASH), evidences the suitability of VA after proper alkaline activation. Moreover, iron may also participate in the formation of new cementitious phases and provide environmental and material performance benefits as reported elsewhere [25]. In addition, the SiO_2/Al_2O_3 molar ratio was computed from the XRF results, being approximately 5.6. Some researchers suggest that the optimum SiO_2/Al_2O_3 molar ratio for the formulation of AABs should be between 3.3 and 4.5 [26]. For higher values, activating solutions with a high Na_2O concentration and curing temperatures close to 80 °C could be required [27].

The mineral and crystalline phases of VA were determined through X-ray diffraction (XRD) using a Bragg–Brentano PANalytical X'Pert PRO MPD alpha1 powder diffractometer device with CuKα1 radiation. It was expected that the mineral phases did not show a weathering process and had not undergone any diagenesis process that could lead to zeolitisation or argillisation of the VA [13] due to the short time elapsed between the eruption of the volcano and the collection of the VA samples. This hypothesis is also supported by the studied VA's low total volatile content (i.e. loss on ignition, LOI). The XRD pattern showed crystalline phases of the inosilicates family, which matches the one described by the contemporary emitted lava flows [1]. Aluminous augite ($Ca(Mg,Al,Fe)Si_2O_6$; #24–0202), diopside ($(Mg_{0.6}Fe_{0.2}Al_{0.2})Ca(Al_{0.5}Si_{1.5})O_6$; #72–1379), and nesosilicates as olivine -forsterite- ($Mg_{1.39}Fe_{0.61}SiO_4$; #79–1201) were detected. In this sense, crystalline iron-bearing phases such as forsterite and augite can form new ferric sites in the structural network [28]. Also, feldspars as anorthite ($Ca(AlSi_2O_8)$; #73–0264) and metallic oxides such as magnetite (Fe_3O_4;

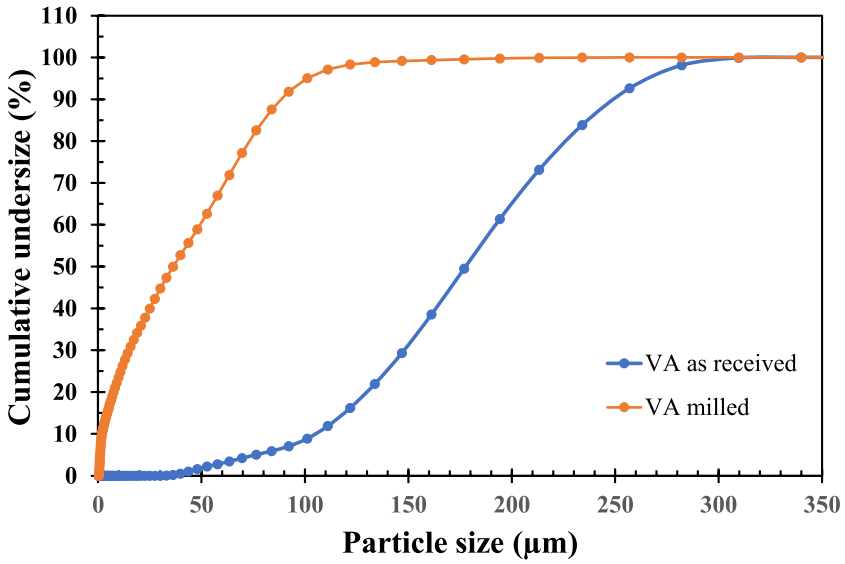

Fig. 2. Particle size distribution of VA as received and after grinding process (VA milled).

Table 1
Major, minor, and trace element composition of VA.

Major and minor elements (wt.%)												
SiO_2	Al_2O_3	Fe_2O_3[a]	CaO	MgO	Na_2O	K_2O	TiO_2	MnO	P_2O_5	S	Cl	LOI[b]
43.36	13.19	13.59	11.60	8.40	3.29	1.42	3.64	0.19	0.77	0.56	0.02	0.51
Trace elements (mg·kg^{-1})												
Ce	**Cr**	**Cu**	**La**	**Nb**	**Nd**	**Ni**	**Sn**	**Sr**	**V**	**Y**	**Zn**	**Zr**
173	377	125	75	72	59	145	32	1042	337	32	120	289

[a] The content of iron is expressed as total iron oxide, calculated by stoichiometry from the iron signal, as usual, is reported for results from XRF spectrometry analysis.
[b] Loss on ignition at 1100 °C.

#80–0390) and titanomagnetite ($(Fe_{2.5}Ti_{0.5})O_4$; #075–1377) were identified. In addition, the amorphous content (Wamorphous) of VA was estimated through the degree of crystallinity (DOC) method [29], following Eq. (1).

$$W_{amorphous} = \left(1 - \frac{Crystalline\ Area}{Crystalline\ Area + Amorhpous\ Area}\right) \cdot 100 \quad \text{Eq. 1}$$

It should be noted that the diffractogram of VA shows an amorphous halo at the 2θ position between 20° and 40° (Fig. 6) due to the rapid air cooling of the VA in the gas plume, which increases the glassy content. Moreover, the grinding process reduced the VA's particle size and increased their specific surface area, enhancing the material's reactivity (mechanical activation) and leading to the amorphisation of the mineral phases [13]. In this case, the amorphous content of the VA from Tajogaite volcano was around 55%, which is much higher than the suggested amorphous phase content (36%) to obtain AABs from VA with adequate properties [15].

Although the content of mineral phases rich in silicates and aluminosilicates is significant in the VA, it is known that crystalline phases are much less reactive than amorphous phases and that temperature and activator concentration are key factors determining the availability of SiO_2 and Al_2O_3 during the gelation stage [30]. Accordingly, the potential availability of reactive phases (SiO_2 and Al_2O_3) was determined through chemical attacks with NaOH solutions (4 M, 6 M, and 8 M). Thus, 1 g of IBA samples was mixed with 100 mL of each activating solution and stirred for 5 h at 80 °C [31]. The resulting solution was filtered and analyzed by inductively coupled plasma optical emission spectrometry (ICP-OES), using PerkinElmer Optima ICP-OES 3200 RL equipment to quantify the Si and Al leached. Fig. 3 shows the potential availability of the gel-forming compounds of the binder phases, SiO_2 and Al_2O_3. The availability of SiO_2 and Al_2O_3 increases with increasing NaOH molarity, except for Al_2O_3 in the 6 M and 8 M attacks, where no significant differences are observed, revealing that the maximum possible amount of SiO_2 and Al_2O_3 has been extracted under the particle size, temperature and time conditions studied.

Fig. 3a shows the percentage of available SiO_2 and Al_2O_3 as a function of the total amount of SiO_2 and Al_2O_3 determined by XRF (Table 1). The results revealed that using 6 M and 8 M NaOH solutions led to a higher extraction (availability) of the SiO_2 and Al_2O_3 contained in the VA (around 33–35 wt%) than using 4 M NaOH (around 25–27%). However, in Fig. 3b, the total SiO_2 and Al_2O_3 availability (g·kg^{-1}) observed between the two gel-forming oxides of the cementitious phases significantly differed due to the difference in their initial content (see Table 1). Thus, the availability results allowed computing the SiO_2/Al_2O_3 molar ratio depending on NaOH molarity, which was 5.2 (4 M), 5.9 (6 M) and 6.1 (8 M), revealing a similar molar ratio than in the initial ratio in VA (5.6) and demonstrating that the higher alkalinity of the NaOH solution, the higher the SiO_2/Al_2O_3 molar ratio of the VA.

Furthermore, the XRD patterns (not shown) of the insoluble fractions obtained from chemical etching to assess the availability of SiO_2 and Al_2O_3 showed the same mineral phases as the initial VA. Although some peaks saw a slight reduction in intensity, a noticeable decrease in the amorphous halo at the 2θ position between 20° and 40° was observed. These observations conclude that the primary phases undergoing activation are the amorphous phases present in the precursor.

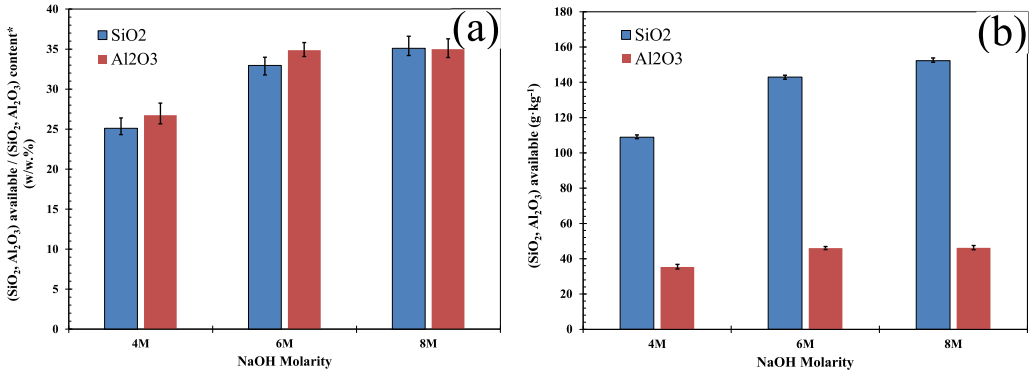

Fig. 3. Availability of SiO_2 and Al_2O_3 resulting from the chemical attacks. (a) wt.%. (b) g·kg^{-1}.

2.3. Samples preparation

The preparation of the alkali-activated VA binders (AA-VA) was conducted by mixing, when necessary, the alkaline activator solutions (Na_2SiO_3/NaOH) for 2 min until a homogeneous activating solution (A) was obtained [32]. Subsequently, the solid precursor VA (P) was gradually added to the liquid for 2 min at 400 rpm to favour the dissolution of reactive phases. The entire mixture was then stirred for 1 min at 700 rpm. Next, the fresh pastes were poured into 25 × 25 × 25 mm silicone cubic moulds and sealed in plastic bags. Finally, all specimens were placed on a vibratory shaker for 5 min at 35 Hz to promote air release from within the cementitious matrix. Nine cubic-shaped specimens were prepared for each formulation. Specimens formulated were subjected to different curing temperatures (room temperature, 40 °C and 60 °C) for 3 days. After this initial curing period, the specimens were demoulded, and the curing stage continued at room temperature and ambient relative humidity. During this short curing period (3 days), setting and consistency were evaluated to rule out some activator solutions, A/P ratios or initial curing conditions. Finally, after 28 days of curing, the specimens were measured and weighed before subsequent testing and analysis to determine their chemical, physical, mechanical, and environmental properties.

2.4. Preliminary studies

Preliminary studies covering a wide range of preparation and curing conditions were conducted to determine an optimal formulation that would meet the mechanical requirements while being as sustainable as possible, given the limited resources available to an island. Table 2 describes these preliminary formulations and the curing conditions of the AABs made using VA (AA-VA) from the Cumbre Vieja ridge eruption as the sole precursor. The selection of the activator solution, as well as the activator–precursor (A/P) ratio and curing conditions, were established based on the results of setting, consistency, workability and pourability of the mixtures obtained in preliminary tests carried out. Moreover, according to SiO_2 and Al_2O_3 availability (see Fig. 3), the 4 M NaOH solution was discarded as an alkaline activator.

Considering the above, different liquid-to-solid (A/P) ratios (0.3, 0.35, 0.4 and 0.5) and curing temperature conditions (room temperature, 40 °C, and 60 °C) were tested. On the one hand, observations of fresh pastes indicated that the liquid-to-solid ratio of 0.4 showed optimum workability and pourability. Lower A/P ratios (i.e. 0.35 and 0.3) showed poor workability and fluidity for adequate pouring into the moulds. In addition, an A/P ratio of 0.5 showed a poor setting of fresh paste or insufficient consistency to be demoulded after 3 days of curing despite its good workability and pourability. On the other hand, as for the curing temperature, the setting and consistency of the specimens formulated with an A/P ratio of 0.4 and cured during the first 3 days at temperatures below 60 °C (i.e. room temperature and 40 °C) was insufficient to be demoulded or did not allow further handling. Finally, regarding the different activating solutions studied, no substantial changes in setting and consistency were noted when using the Na_2SiO_3 solution. Therefore, it was decided to use 6 M and 8 M NaOH solutions as alkaline activators due to their lower carbon footprint compared to Na_2SiO_3.

2.5. Characterization of alkali-activated VA binders (AA-VA)

Hydrolytic stability was evaluated by immersing one of the specimens obtained from each formulation in boiling water for 20 min [33]. Then, a visual assessment was conducted to identify any possible dissolution of binder components and monitor the overall structural cohesion. Finally, the specimens were dried in a desiccator and weighed to determine the mass loss and water stability.

The mineral and crystalline phases of the cured specimens were analyzed using XRD. The vibrational energies of the most characteristic bonds in the formulated binders were identified through Fourier-transform infrared spectroscopy (FT-IR) using the attenuated total reflectance (ATR) method in a Spectrum Two™ PerkinElmer spectrometer. Although the measures were carried out in the range of 4000–500 cm^{-1} with a resolution of 4 cm^{-1}, the study was focused mainly on the 1200-800 cm^{-1} range corresponding to the symmetric and asymmetric stretching vibrations of Si–O bonds [34]. The microstructure and microstructural analysis of AABs formulated was conducted using a scanning electron microscopy (SEM) device (ESEM FEI Quanta 200) with energy dispersive X-ray spectroscopy (EDS).

The compressive strength at 3, 7 and 28 days of curing was determined for each formulation by testing three cubic specimens according to UNE-EN 196–1. An Incotecnic MULTI-R1 was used, equipped with a 20 kN load cell and used to apply a progressive load

Table 2
Preliminary formulations of AA-VA.

	Liquid-to-solid ratio (A/P)	Sodium hydroxide (NaOH)		Sodium Silicate (Na_2SiO_3)	Curing Temperature
		Molarity	(% of A)	(% of A)	
PS.1	0.5	8 M	100%	0%	Room
PS.2	0.4	8 M	100%	0%	Room
PS.3	0.4	8 M	50%	50%	Room
PS.4	0.4	8 M	50%	50%	60 °C
PS.5	0.4	8 M	30%	70%	Room
PS.6	0.4	8 M	30%	70%	60 °C
PS.7	0.4	6 M	30%	70%	60 °C
PS.8	0.4	6 M	50%	50%	60 °C
PS.9	0.4	6 M	100%	0%	60 °C
PS.10	0.3	6 M	100%	0%	60 °C
PS.11	0.35	6 M	100%	0%	40 °C

until fracture (loading rate of 240 kg s^{-1}). The apparent density was determined by measuring and weighing the prismatic samples after 3, 7 and 28 days of curing.

The potential release of heavy metals and metalloids from AAB specimens was evaluated through a granular leaching test following European standard EN 12547–4. An ICP-MS (Inductively Coupled Plasma Mass Spectrometry) device from Perkin-Elmer ELAN 6000 was used to analyze the heavy metals and metalloids in the eluates, including As, Ba, Cd, Cr, Cu, Hg, Mo, Pb, Ni, Se, Sb, and Zn. Two replicates were conducted for each binder formulation.

3. Results and discussion

No significant differences were observed in the hydrolytic stability of the specimens with a proper setting and consistency (i.e. A/P = 0.4 and 60 °C curing temperature). Furthermore, after the hydrolytic stability test, all of the tested specimens remained cohesive and did not disaggregate, and the weight loss was less than 2%, which was insufficient to affect their structural consistency.

Fig. 4 shows the micrographs of a cross-section of specimens formulated with an A/P ratio of 0.4 and cured at 60 °C, taken in backscattered electron (BSE) mode using a scanning electron microscope (SEM) at two different magnifications. The contrast in the resulting images allows for easy identification of the solid cementitious matrix, the unreacted VA particles and the pores (black colour). These low-reactivity mineral phases of VA act as fine aggregates and remain almost unchanged, providing increased cohesion and mechanical strength. As a result, the formulated AABs can be considered micro-mortar-like materials that consist of cementitious phases and homogeneously distributed fillers throughout the binder matrix. When examining porosity, it can be seen in the lower magnification micrographs (Fig. 4a and b) that, while the differences are not substantial, the formulation made with 8 M NaOH exhibits similar porosity.

As a complementary study to the micrographs displayed previously, Fig. 5 shows an elemental mapping acquired from the same areas as the BSE micrograph after two 6 min-cycles of the specimen formulated using 6 M NaOH as an alkaline activator, obtained by SEM-EDS. The mapping shows the distribution of elements such as Si, Al, Ca and Na within the specimen, at high magnification.

BSE micrograph (grayscale) of the specimen provides details about the microstructure and morphology of the specimen. Again, unreacted VA particles can be observed embedded in a cementitious matrix, similar to what could be a micromortar in which the particles act as a micro-aggregate. The red scale mapping (Na) also outlines the boundary between the VA particles and the cementitious matrix. As expected, since no sodium-containing mineral phases were found in the VA and the only source of this element is the activator, the sodium is present only in the cementitious matrix. However, the calcium (blue scale) presence in the cementitious matrix is lower than the one observed for Na. There are even some areas of the binder where no calcium is present or is found in low concentrations. As for the elemental map in green scale, aluminium appears homogenously distributed throughout the specimen, with no significant differences between the particles and the cementitious matrix. In contrast, the silicon content in the unreacted particles (yellow scale) is higher than in the cementitious matrix, since most of the crystalline phases observed through XRD in the VA were silicates or aluminosilicates. These observations are consistent with the results of the availability analysis determined by the chemical

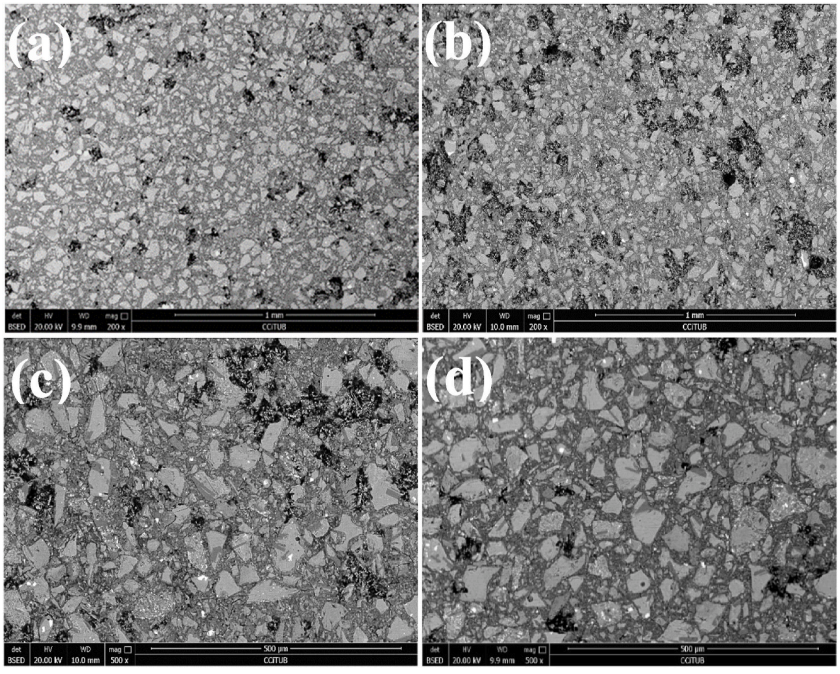

Fig. 4. SEM micrographs of a cross-section of the specimens taken in backscattered electron (BSE) mode at two different magnifications. A/P ratio of 0.4 and curing temperature of 60 °C. (a), (c) 6 M NaOH and (b), (d) 8 M NaOH.

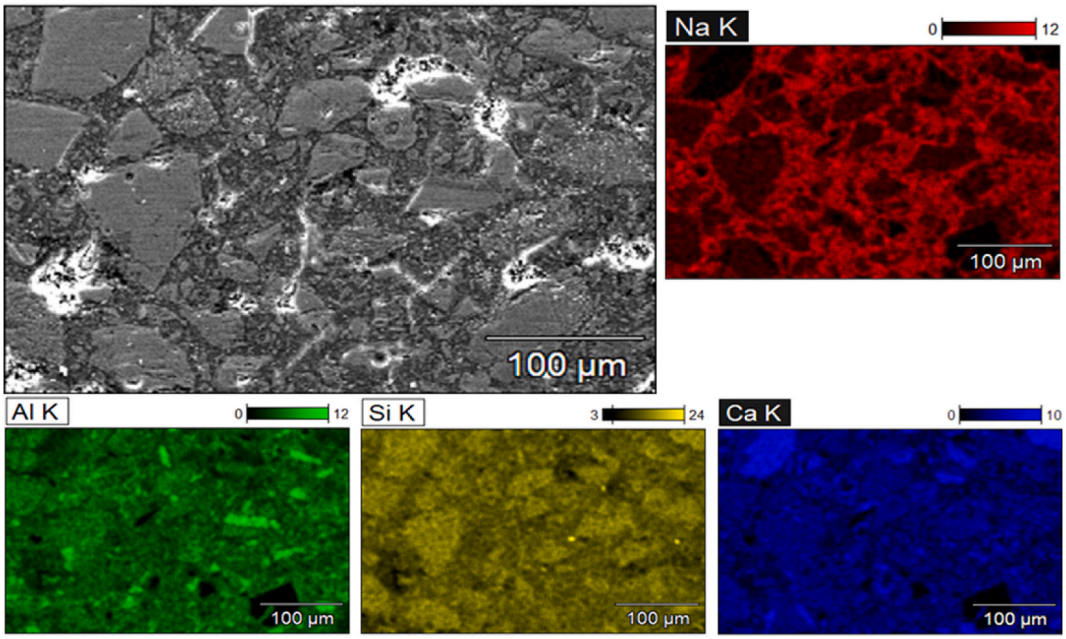

Fig. 5. SEM backscattered electron (BSE) micrograph (grayscale) and EDS elemental (K_α) maps (red scale: Na; green scale: Al; yellow scale: Si; blue scale: Ca) of the AAB specimen formulated using 6 M NaOH solution as the activator. (For interpretation of the references to colour in this figure legend, the reader is referred to the Web version of this article.)

attack (Fig. 3), which suggested that aluminium is the limiting element for forming the binder gels. Therefore, even though the calcium content in the mineral phases of VA is high (see Table 1), it can be expected that the cementitious matrix is mainly composed of NASH or (N,C)ASH gels, while CASH and CSH structures should be found in low proportions.

Fig. 6 shows the diffractograms of the VA sample and AA-VA binders, and Table 3 summarises the main crystalline phases identified. As evident from the analysis, certain mineral phases identified in the VA sample were also determined in the two formulated binders (i.e. anorthite, olivine, and magnetite). This finding revealed that some unreacted VA mineral phases and/or particles persist in the binder materials, embedded within the cementitious matrix, and functioning as fillers. In addition, mineral phases that were generated through alkaline activation, such as sodium-rich anorthite (anorthite, sodian) and aluminium-rich augite (augite, aluminan), have been identified. In these phases, the activating cation and/or aluminium from other VA mineral phases have been

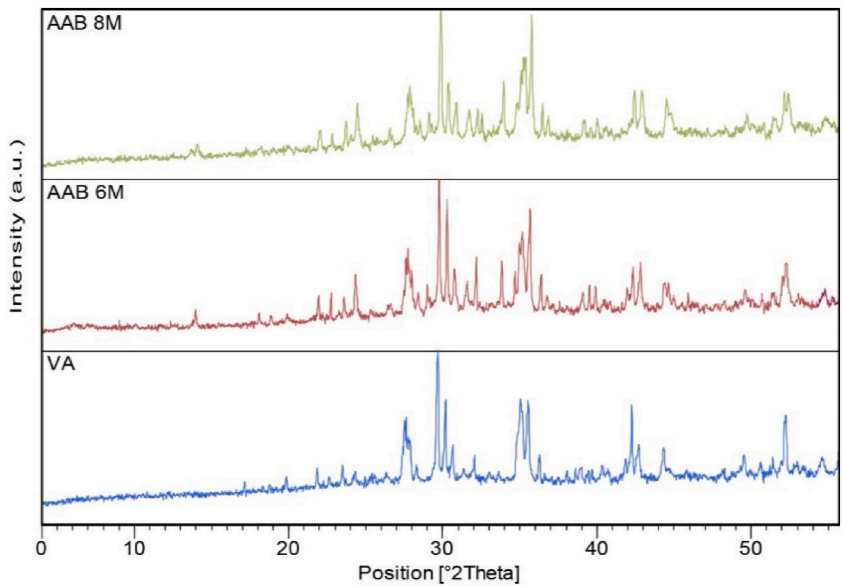

Fig. 6. X-ray diffraction (XRD) patterns of volcanic ash (VA) and alkali-activated binders (AAB) formulated using VA as a sole precursor and 6 M and (M NaOH as activator solution, respectively.

Table 3
The main crystalline and mineral phases, identified by XRD, of VA and alkali-activated binders formulated using VA as the sole precursor and 6 M and 8 M NaOH as the activator solution.

Identified phase		Ref. Code	VA	AAB 6 M	AAB 8 M
Anorthite	$Ca(Al_2Si_2O_8)$	01-073-0265	✓		✓
Anorthite, sodian	$(Ca,Na)\ (Al,Si)_2\ Si_2\ O_8$	00-009-0465		✓	✓
Augite	$Ca(Mg,Fe)Si_2O_6$	00-024-0203	✓		
Augite, aluminan	$Ca(Mg,Fe,Al)\ (Si,\ Al)_2O_6$	00-041-1483		✓	✓
Olivine	$(Mg,Fe)SiO_2$	01-079-1203	✓	✓	✓
Magnetite	Fe_3O_4	01-089-0951	✓	✓	✓
Trona	$Na_3H(CO_3)_2\ (H_2O)_2$	01-078-1064		✓	✓
Corderoite	$Hg_3S_2Cl_2$	01-074-2121		✓	
Fueloppite	$Pb_3Sb_8S_{15}$	00-022-0648			✓

introduced into the crystal lattice of the precursor phases. These neoformed mineral phases are associated with the secondary products generated during the gelation of NASH and (N,C)ASH gels. Also, note the presence of trona ($Na_3H(CO_3)_2{\cdot}(H_2O)_2$) in both binders as a result of the carbonation of the activator (NaOH) through atmospheric CO_2. Finally, two sulfur phases have been identified in the AABs, likely present in the unreacted VA and whose relative content after activation allows them to be identified by XRD.

Fig. 7 depicts the FTIR spectra of the precursor (VA) and the AA-VA binders to compare and determine the formation of the main reaction products and cementitious phases. The characterization was primarily focused on the most prominent peaks associated with O–C–O bonds and the mid-wavenumber region's broadband (1200-800 cm^{-1}), which is associated with asymmetric stretching vibrations of Si–O-T (where T represents Si or Al). The spectra of the binder material specimens exhibit a broad band above 1405 cm^{-1} attributed to carbonates. It differs from the precursor (VA) spectrum and is a result of the carbonation reaction between the activator (NaOH) and atmospheric CO_2. This event also justifies the appearance of a peak at 868 cm^{-1}, also attributed to the formation of carbonates during the first curing stages of the formulated binders. In the mid-wavenumber region (1200–800 cm^{-1}), the vibrational motion is mainly attributed to the asymmetric stretching and bending vibrational modes of the Si–O bond, which results in a shift in the bond length and a change in the bond strength. This stretching vibration is characterised by broadband, where its specific frequency can depend on the chemical environment of the Si–O bond, such as the presence of neighbouring atoms or the chemical structure. Thus, the absorption bands can change both in position and shape as the content of other elements varies (i.e. Mg, Ca, Fe, Ti or Al). As seen in the FTIR spectrum of the precursor (VA), in the mid-wavenumber region, broadband results from overlapping various peaks corresponding to the stretching and bending vibrations of the Si–O-T bonds (T = Si or Al). The deconvolution of this band does not provide any specific information about the different overlapping peaks due to the nature of the different mineral phases that compose the VA and the large number of chemical elements that can be part of the siliceous structure of these phases; both in interstitial and substitutional positions of Si. However, in the FTIR spectra of the formulated binders (AAB 6 M and AAB 8 M), it is noticeable that the band centred above 965 cm^{-1} is narrower and more prominent. This indicates a change in structure due to the formation of NASH or (N,C)ASH gels, which results in a shift in the peaks related to the vibrations of the Si–O-T bond (T = Si or Al) and the Al–OH bond, as well as the introduction of sodium into the siliceous structure of the binder (i.e. 1140, 1056 and 965 cm-1 bands). It should also be noted that this band has no significant differences between the two binders formulated with different activator concentrations.

The mechanical behaviour of AA-VA binders has been determined by the variation of the compressive strength (σ_c) during the early curing period (3, 7 and 28 days), as shown in Fig. 8. The compressive strength showed a consistent increase over time during the initial curing period as demonstrated by the experimental trials. The 6 M NaOH activation shows higher compressive strength than 8 M NaOH, except for the first three days of curing. The higher compressive strength values observed in the specimens activated with 6 M NaOH solution may be attributed to the higher content of binder phases formed during gelation or to the lower porosity resulting from the formulation with 8 M NaOH solution, as suggested by the observation of the micrographs of both SEM specimens (Fig. 4). This increase with curing time was particularly pronounced in the formulation activated with a 6 M NaOH solution, which resulted in maximum compressive strength of 16.5 MPa after 28 days of curing.

The apparent density of alkali-activated binder specimens formulated using VA as the sole precursor is depicted in Fig. 9. The apparent density slightly decreases (between 7 and 10%) with the curing days in these first 28 days. This fact can be attributed to both the porosity generated from the evaporation of kneading water during chemical activation and the expansion of the samples resulting from the hydration of formed binder phases. However, contrary to what could be expected from the observations of porosity (Fig. 4) and compressive strength (Fig. 7), the apparent density of the binders activated with an 8 M NaOH solution is higher than those obtained with a 6 M NaOH solution. This fact can be explained by the carbonation of the unreacted sodium that remains in the cementitious matrix. In this case, as the sodium content is higher in the 8 M NaOH activator solution, the formation of sodium carbonates is expected to also be higher in the binders formulated with this activator solution. However, despite increasing mass per unit volume, sodium carbonates lack binding properties, thus not improving mechanical properties.

EN 12457-4 standard leaching test was performed to evaluate the potential environmental impact of AABs formulated with IBA as the sole precursor at the end of their lifecycle. Table 4 summarises the leaching concentration of heavy metals and metalloids from precursor (VA) and tested formulations. Increased activator concentration generally leads to increased metal concentrations in the leachate. Moreover, as expected, the heavy metals leached from the formulated specimens are higher than those leached from the precursors due to the aggressive attack carried out at the high pH of the alkaline activating solution. Despite this, all metals and metalloids, except for chromium and molybdenum, have leachate concentrations below the threshold for classification as inert waste.

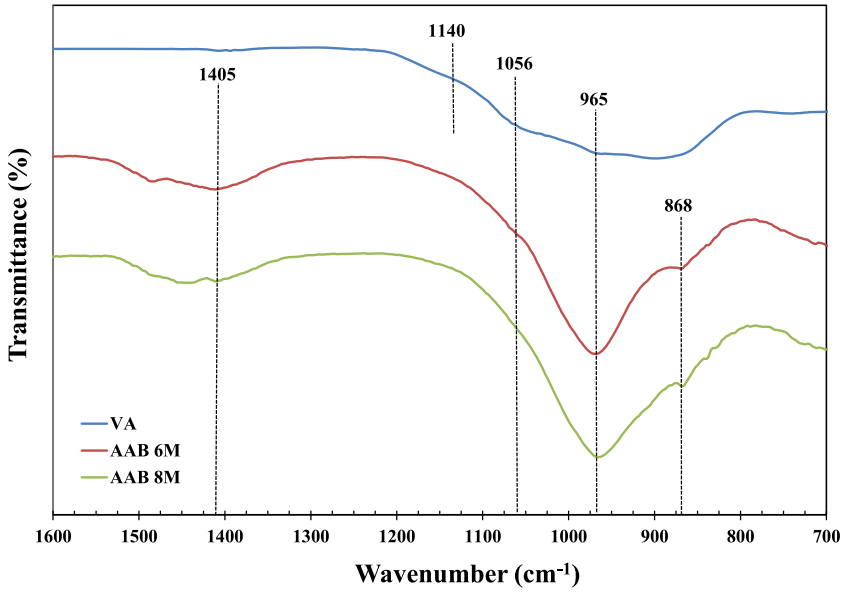

Fig. 7. FT-IR spectra of alkali-activated binders using VA as the sole precursor, formulated using 6 M and 8 M NaOH as the activator.

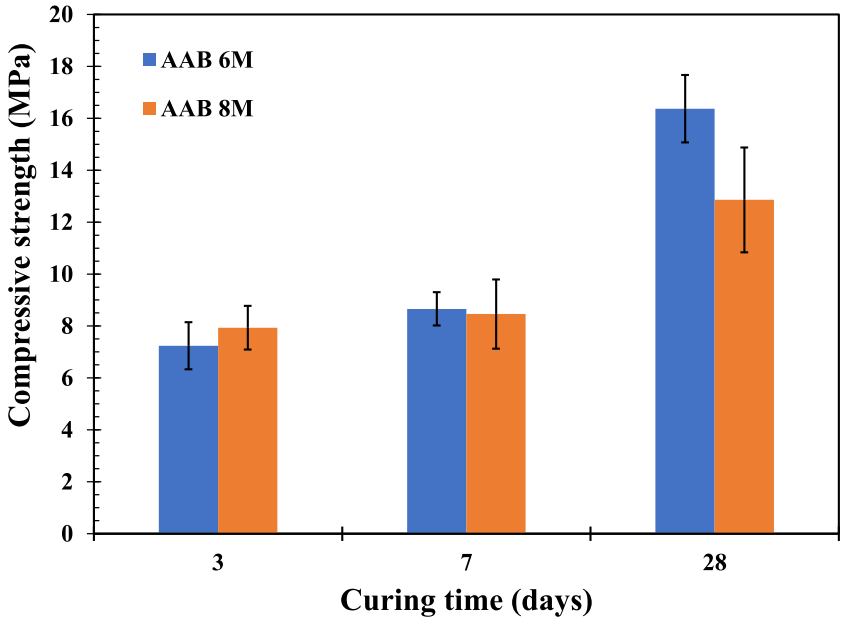

Fig. 8. Compressive strength (σ_c) alkali-activated binders formulated using VA as the sole precursor and 6 M and 8 M NaOH as activator solutions.

Based on these leaching results, AA-VA binders can be considered non-hazardous waste at the end of their life cycle.

4. Conclusions

The volcanic ash (VA) from the Cumbre Vieja ridge eruption is suitable for use as the sole precursor in the formulation of alkali-activated binders. Using locally sourced volcanic ash reduces dependence on imported materials, cuts transportation costs, and lowers the carbon emissions associated with transportation. Additionally, it promotes local economic growth by creating jobs and utilizing local resources.

Prior research found that using a concentrated NaOH activator solution, an activator-to-precursor ratio of 0.4, and a temperature of 60 °C effectively optimized workability, pourability, setting time, and consistency in alkaline binders. Likewise, activation of VA using only concentrated NaOH solutions instead of a Na_2SiO_3/NaOH mixed solution reduces reagent costs and improves the sustainability of the formulation process of alkali-activated binders.

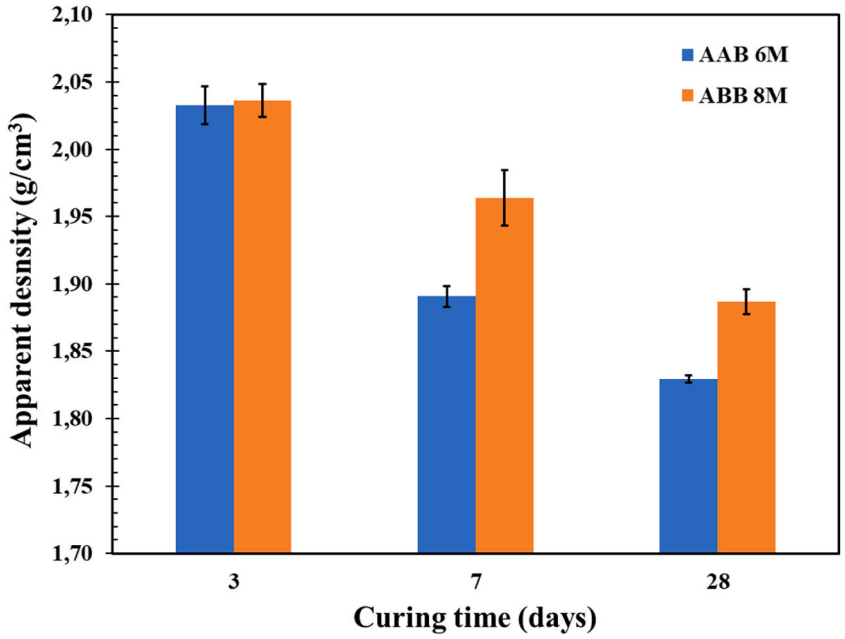

Fig. 9. Apparent density of alkali-activated binders formulated using VA as the sole precursor and 6 M and 8 M NaOH as activator solutions.

Table 4
Leaching test (EN 12457–4). Leaching concentration (mg·kg^{-1}) of VA and alkali-activated binders formulated using 6 M and 8 M NaOH solutions as activators.

	Zn	Pb	Ni	Cr	Cu	Ba	As	Cd	Sb	Mo	Hg
VA	0.26	0.01	0.07	0.03	0.19	0.01	0.01	<0.001	0.02	0.06	<0.01
AAB-6M	<0.20	0.03	<0.02	1.60	0.10	0.03	0.03	<0.010	0.04	2.68	0.01
AAB8M	<0.20	0.03	<0.02	1.32	0.29	0.02	0.03	<0.010	0.03	2.97	0.01
[a]Inert	4	0.5	0.4	0.5	2	20	0.5	0.04	0.06	0.5	0.01
[a]Non-hazardous	50	10	10	10	50	100	2	1	0.7	10	0.2
[a]Hazardous	200	50	40	70	100	300	25	5	5	30	2

[a] Limit for waste acceptance at landfills [35].

The chemical and structural characterization of the binder specimens activated with 6 M and 8 M NaOH solutions did not yield significant differences. In all the formulated specimens, unreacted VA particles were embedded in the matrix, acting as fillers and reinforcing the binder material. However, the best compressive strength (16.5 MPa) after 28 days of curing and the environmental risk (EN 12457-2 leaching test) of alkali-activated binders formulated using volcanic ash as the only precursor was obtained using a 6 M NaOH activator solution.

Credit authorship contribution statement

J. Mañosa: investigation, formal analysis, writing – review & editing; **J. Serrano-Conte**: investigation, writing – review & editing; **A. Maldonado-Alameda**: investigation, validation, writing – review & editing; **M. Aulinas**: resources, validation; **J.M. Chimenos**: conceptualization, methodology, supervision, writing - original draft, funding acquisition.

Funding

This work is partially supported by the Grants PID2021-125810OB-C21 and TED2021-129718B–I00, funded by MCIN/AEI/10.13039/501100011033, by "ERDF A way of making Europe" and by the "European Union NextGenerationEU/PRTR", and the Agència de Gestió d'Ajuts Universitaris i de Recerca (AGAUR) with the Grant 2021 SGR 00708. Furthermore, the Agència de Gestió d'Ajuts Universitaris i de Recerca (AGAUR) also contributed through Mr Jofre Mañosa's PhD grant (FI-DGR 2020).

Declaration of competing interest

The authors declare that they have no known competing financial interests or personal relationships that could have appeared to influence the work reported in this paper.

Data availability

Data will be made available on request.

Acknowledgements

The authors would like to thank the Catalan Government for the quality accreditation given to their research group DIOPMA (2021 SGR 00708). DIOPMA is a certified agent TECNIO in the category of technology developers from the Government of Catalonia. The authors are grateful to Dr Francisco J. Pérez-Torrado and Dr Alejandro Rodríguez-González of the Instituto de Estudios Ambientales y Recursos Naturales (i-UNAT) at the University of Las Palmas de Gran Canaria (ULPGC), Spain, for the supply of volcanic ash.

References

[1] J.C. Carracedo, V.R. Troll, J.M.D. Day, H. Geiger, M. Aulinas, V. Soler, F.M. Deegan, F.J. Perez-Torrado, G. Gisbert, E. Gazel, A. Rodriguez-Gonzalez, H. Albert, The 2021 eruption of the Cumbre Vieja volcanic ridge on La Palma, Canary Islands, Geol. Today 38 (2022) 94–107, https://doi.org/10.1111/gto.12388.
[2] Copernicus, European Union Earth Observer Program, 2022. https://www.copernicus.eu/en/news/news/observer-copernicus-eyes-la-palma-eruption. (Accessed 19 October 2022).
[3] J.M.D. Day, V.R. Troll, M. Aulinas, F.M. Deegan, H. Geiger, J.C. Carracedo, G.G. Pinto, F.J. Perez-Torrado, Mantle source characteristics and magmatic processes during the 2021 La Palma eruption, Earth Planet Sci. Lett. 597 (2022), 117793, https://doi.org/10.1016/j.epsl.2022.117793.
[4] World wide Cement production 2018 & forecast 2030, world Cement association. https://www.worldcementassociation.org/wca-media/infographics.
[5] R.M. Andrew, Global CO2 emissions from cement production, Earth Syst. Sci. Data 10 (2018) 195–217, https://doi.org/10.5194/essd-10-195-2018.
[6] J.L. Provis, Geopolymers and other alkali activated materials: why, how, and what? Mater. Struct. 47 (2014) 11–25, https://doi.org/10.1617/s11527-013-0211-5.
[7] J.L. Provis, J.S.J. van Deventer, Alkali Activated Materials: State-Of-The-Art Report, RILEM TC 224-AAM, Springer Netherlands, 2013.
[8] T. Adeoti, C. Fantini, G. Morgan, S. Thacker, P. Ceppi, N. Bhikhoo, S. Kumar, S. Crosskey, N. O'Regan, Infrastructure for Small Island Developing States, Copenhagen, Denmark, 2020. https://content.unops.org/publications/Infrastructure_SIDS_EN.pdf.
[9] C. Leonelli, E. Kamseu, D.N. Boccaccini, U.C. Melo, A. Rizzuti, N. Billong, P. Miselli, Volcanic ash as alternative raw materials for traditional vitrified ceramic products, Adv. Appl. Ceram. 106 (2007) 135–141, https://doi.org/10.1179/174367607X159329.
[10] M.D. Sleep, M. Masley, The use of Mt. Mazama volcanic ash as natural pozzolans for sustainable soil and unpaved road improvement. https://rosap.ntl.bts.gov/view/dot/37447.
[11] P.N. Lemougna, K. tuo Wang, Q. Tang, A.N. Nzeukou, N. Billong, U.C. Melo, X. min Cui, Review on the use of volcanic ashes for engineering applications, Resour. Conserv. Recycl. 137 (2018) 177–190, https://doi.org/10.1016/j.resconrec.2018.05.031.
[12] J. Rosales, M. Rosales, J.L. Díaz-López, F. Agrela, M. Cabrera, Effect of processed volcanic ash as active mineral addition for Cement manufacture, Materials 15 (2022) 6305, https://doi.org/10.3390/ma15186305.
[13] A. Játiva, E. Ruales, M. Etxeberria, Volcanic ash as a sustainable binder material: an extensive review, Materials 14 (2021) 1–32, https://doi.org/10.3390/ma14051302.
[14] P.N. Lemougna, K.J.D. MacKenzie, U.F.C. Melo, Synthesis and thermal properties of inorganic polymers (geopolymers) for structural and refractory applications from volcanic ash, Ceram. Int. 37 (2011) 3011–3018, https://doi.org/10.1016/j.ceramint.2011.05.002.
[15] H.K. Tchakoute, A. Elimbi, E. Yanne, C.N. Djangang, Utilization of volcanic ashes for the production of geopolymers cured at ambient temperature, Cement Concr. Compos. 38 (2013) 75–81, https://doi.org/10.1016/j.cemconcomp.2013.03.010.
[16] M.I. Khan, A.M. Alhozaimy, Properties of natural pozzolan and its potential utilization in environmental friendly concrete, Can. J. Civ. Eng. 38 (2010) 71–78, https://doi.org/10.1139/L10-112.
[17] P.N. Lemougna, U.F. Chinje Melo, M.P. Delplancke, H. Rahier, Influence of the activating solution composition on the stability and thermo-mechanical properties of inorganic polymers (geopolymers) from volcanic ash, Construct. Build. Mater. 48 (2013) 278–286, https://doi.org/10.1016/j.conbuildmat.2013.06.089.
[18] T. Huang, S.-W. Zhang, L. Zhou, A. Li, H. Tao, Self-cementation of the alkali-activated volcanic tuff coupling with thiol-functionalized expanded perlite that enhances the solidification and stabilization of the mercury-contaminated soil, Chem. Eng. J. 428 (2022), 131059, https://doi.org/10.1016/j.cej.2021.131059.
[19] D. Song, T. Huang, Q. Fang, A. Liu, Y.-F. Gu, Y.-Q. Liu, L.-F. Liu, S.-W. Zhang, Feasibility exploration on the geopolymerization activation of volcanic tuff, parametrical optimization, and reaction mechanisms, J. Mater. Res. Technol. 11 (2021) 618–632, https://doi.org/10.1016/j.jmrt.2021.01.029.
[20] J.N.Y. Djobo, A. Elimbi, H.K. Tchakouté, S. Kumar, Volcanic ash-based geopolymer cements/concretes: the current state of the art and perspectives, Environ. Sci. Pollut. Control Ser. 24 (2017) 4433–4446, https://doi.org/10.1007/s11356-016-8230-8.
[21] N.M. Martín Lorenzo, D. A., Andronico, F. Rodríguez, B. Coldwell, M. Pankhurst, J. Taddeucci, P. Scarlato, C. Bonadonna, M. Pistolesi, J.E. Romero, G. Melián, Pérez, Preliminary results from textural studies on tephra deposits erupted during the 2021 eruption at Cumbre Vieja volcano, in: EGU General Assembly Conference 2022, Vienna, Austria, 2022, p. 9986, https://doi.org/10.5194/egusphere-egu22-9986, 2022.
[22] J.E. Romero, M. Burton, F. Cáceres, J. Taddeucci, R. Civico, T. Ricci, M.J. Pankhurst, P.A. Hernández, C. Bonadonna, E.W. Llewellin, M. Pistolesi, M. Polacci, C. Solana, L. D'Auria, F. Arzilli, D. Andronico, F. Rodríguez, M. Asensio-Ramos, A. Martín-Lorenzo, C. Hayer, P. Scarlato, N.M. Perez, The initial phase of the 2021 Cumbre Vieja ridge eruption (Canary Islands): products and dynamics controlling edifice growth and collapse, J. Volcanol. Geoth. Res. 431 (2022), 107642, https://doi.org/10.1016/j.jvolgeores.2022.107642.
[23] M.A. Riseh, M.V. Abedini, M.H. Emami, S.J.S. Zakariaei, M.A. Riseh, M.V. Abedini, M.H. Emami, S.J.S. Zakariaei, The petrography, mineralography and microprobe analysis on new exploratory excavation phase in Sarcheshmeh copper mine pit and Comparing them with existing data from the other area in South West Sarcheshmeh, Open J. Geol. 7 (2017) 162–181, https://doi.org/10.4236/ojg.2017.72011.
[24] J.M.D. Day, H. Geiger, V.R. Troll, F.J. Perez-Torrado, M. Aulinas, G. Gisbert, J.C. Carracedo, Bouncing Spallation bombs during the 2021 La Palma eruption, Canary Islands, Spain, Earth Science, Systems and Society 2 (2022). https://www.escubed.org/articles/10.3389/esss.2022.10063.
[25] V. Ponomar, J. Yliniemi, E. Adesanya, K. Ohenoja, M. Illikainen, An overview of the utilisation of Fe-rich residues in alkali-activated binders: mechanical properties and state of iron, J. Clean. Prod. 330 (2022), 129900, https://doi.org/10.1016/j.jclepro.2021.129900.
[26] P.N. Lemougna, K. Wang, Q. Tang, U.C. Melo, X. Cui, Recent developments on inorganic polymers synthesis and applications, Ceram. Int. 42 (2016) 15142–15159, https://doi.org/10.1016/j.ceramint.2016.07.027.
[27] B.I. Djon Li Ndjock, A. Elimbi, M. Cyr, Rational utilization of volcanic ashes based on factors affecting their alkaline activation, J. Non-Cryst. Solids 463 (2017) 31–39, https://doi.org/10.1016/j.jnoncrysol.2017.02.024.
[28] P.N. Lemougna, K.J.D. MacKenzie, G.N.L. Jameson, H. Rahier, U.F. Chinje Melo, The role of iron in the formation of inorganic polymers (geopolymers) from volcanic ash: a 57Fe Mössbauer spectroscopy study, J. Mater. Sci. 48 (2013) 5280–5286, https://doi.org/10.1007/s10853-013-7319-4.
[29] I.C. Madsen, N.V.Y. Scarlett, A. Kern, Description and survey of methodologies for the determination of amorphous content via X-ray powder diffraction, Z. Kristallogr. 226 (2011) 944–955, https://doi.org/10.1524/zkri.2011.1437.
[30] C. Ruiz-Santaquiteria, A. Fernándes-Jiménez, A. Palomo, Quantitative determination of reactive SiO2 and Al2O3 in aluminosilicate materials, 13th International Congress on the Chemistry of Cement (2011) 1–7.
[31] C. Kuenzel, N. Ranjbar, Dissolution mechanism of fly ash to quantify the reactive aluminosilicates in geopolymerisation, Resour. Conserv. Recycl. 150 (2019), 104421, https://doi.org/10.1016/j.resconrec.2019.104421.

[32] B. Skariah Thomas, J. Yang, A. Bahurudeen, S.N. Chinnu, J.A. Abdalla, R.A. Hawileh, H.M. Hamada, Geopolymer concrete incorporating recycled aggregates: a comprehensive review, Cleaner Materials 3 (2022), 100056, https://doi.org/10.1016/j.clema.2022.100056.
[33] W. Zhu, X. Chen, L.J. Struble, E.H. Yang, Characterization of calcium-containing phases in alkali-activated municipal solid waste incineration bottom ash binder through chemical extraction and deconvoluted Fourier transform infrared spectra, J. Clean. Prod. 192 (2018) 782–789, https://doi.org/10.1016/j.jclepro.2018.05.049.
[34] Y. Ping, R.J. Kirkpatrick, P. Brent, P.F. McMillan, C. Xiandong, Structure of Calcium silicate hydrate (C-S-H): near-, mid-, and far-Infrared spectroscopy, J. Am. Ceram. Soc. 82 (1999) 742–748, https://doi.org/10.1111/j.1151-2916.1999.tb01826.x.
[35] Council of the European Union, 2003/33/EC, Council Decision Establishing Criteria and Procedures for the Acceptance of Waste at Landfills Pursuant to Article 16 of and Annex II to Directive 1999/31/EC, Official Journal of the European Communities, 2003, pp. 27–49.